JOURNAL OF CATALYSIS 154, 124–136 (1995)

Non-Faradaic Electrochemical Modification of Catalytic Activity

VIII. Rh-Catalyzed C_2H_4 Oxidation

C. Pliangos, I. V. Yentekakis, X. E. Verykios, and C. G. Vayenas[1]

Department of Chemical Engineering, University of Patras, Patras GR-26500, Greece

Received August 1, 1994; revised January 13, 1995

The catalytic activity of polycrystalline Rh films deposited on 8 mol% Y_2O_3-stabilized ZrO_2 (YSZ), an O^{2-} conductor, can be altered dramatically and reversibly by varying the potential of the Rh catalyst film. The complete oxidation of ethylene was investigated as a model reaction in the temperature range 300 to 400°C and at atmospheric total pressure. The rate of C_2H_4 oxidation can be reversibly enhanced by up to 100 times by supplying O^{2-} to the catalyst via positive potential application (up to 1.5 V). This is the highest rate enhancement observed so far with *in situ* electrochemical promotion studies. The steady-state rate increase is typically 10^4 times larger than the steady-state rate of O^{2-} supply to the catalyst. It was also found that varying the catalyst potential causes the appearance of the well-known compensation effect with an isokinetic point at 372°C. As in previous studies of the effect of non-Faradaic electrochemical modification of catalytic activity (NEMCA) the observed behaviour is due to the promotional action of back-spillover oxide ions which migrate from the YSZ solid electrolyte onto the catalyst surface under the influence of the applied potential. The back-spillover oxide ions are less reactive with C_2H_4 than normally chemisorbed oxygen and act as promoters by affecting the binding strength of chemisorbed oxygen and ethylene.

INTRODUCTION

Rhodium is an important constituent of three-way automotive exhaust catalysts and its interaction with oxygen (1–3), NO (4–7), CO (8–12), and light hydrocarbons (13, 14) has been the focal point of numerous UHV investigations (1–14) and atmospheric pressure kinetic studies (15–19). The interaction of Rh with oxygen, in particular, has attracted considerable attention due to the fact that under real catalytic conditions an excess of oxygen results in significant deactivation and oxide formation (15, 16). Due to its high cost, a reduction in the amount of Rh present in automotive exhaust catalytic converters, via appropriate promotion of its catalytic properties, would be highly desirable.

[1] To whom correspondence should be addressed.

During the last six years the effect of non-Faradaic electrochemical modification of catalytic activity (NEMCA) (20–39), electrochemical promotion (40), or *in situ* controlled promotion of catalyst surfaces (41) has been described for over 25 catalytic reactions on Pt, Pd, Ag, and Ni surfaces using O^{2-}-conducting solid electrolytes, such as yttria-stabilized zirconia (YSZ) (20–28, 33–39); Na^+-conducting solid electrolytes, such as β''-Al_2O_3 (20, 29, 41, 42); H^+-conducting solid electrolytes, such as $CsHSO_4$ (38); and F^--conducting solid electrolytes, such as CaF_2 (43), as the active catalyst support. Work prior to 1992 has been reviewed (21). The effect has also been recently demonstrated in aqueous electrolyte systems (44).

The porous metal catalyst film also serves as an electrode in the galvanic cell

gaseous reactants, metal catalyst/solid electrolyte/metal, O_2

and the NEMCA effect is induced by applying currents or potentials (typically −2 to +2 V) between the catalyst film and the metal counter electrode (20, 21). The induced change in catalytic rate on the catalyst film is up to 3×10^5 times higher than the rate of ion supply (21, 24) and, until the present study, up to 70 times higher than the catalytic rate when no voltage is applied (21, 24).

When YSZ is used as the solid electrolyte, NEMCA is due to the promoting action of spillover oxide ions $O^{\delta-}$ as originally proposed (21, 24) and as recently confirmed by XPS (45). The promoting oxide ion on Pt has an O 1*s* binding energy of 528.8 eV vs 530.0 eV for normally chemisorbed oxygen which coexists on the surface (45). The enhancement factor or Faradaic efficiency, Λ, is defined by

$$\Lambda = \Delta r/(I/2F), \qquad [1a]$$

where Δr is the induced change in catalytic rate expressed in mol O/s; I is the applied current, defined as positive

0021-9517/95 $6.00

when anions are supplied to the catalyst; and F is Faraday's constant. More generally, Λ can be defined from

$$\Lambda = \Delta r'/(I/F), \qquad [1b]$$

where r' is expressed in g-equivalent/s. A reaction exhibits the NEMCA effect when $|\Lambda| > 1$. When $\Lambda > 1$ the reaction is termed electrophobic, while when $\Lambda < -1$ the reaction is termed electrophilic.

When β''-Al_2O_3 is used as the solid electrolyte, NEMCA is due to the promoting action of spillover $Na^{\delta+}$ (29, 41). The coverage θ_{Na} of sodium on the catalyst surface can be easily measured coulometrically (41). In such cases a very useful parameter is the promotion index P_i defined by (41),

$$P_i = \frac{\Delta r/r_0}{\Delta\theta_i}, \qquad [2]$$

where r_0 is the unpromoted catalytic reaction rate and θ_i is the coverage of the promoting species (e.g., $Na^{\delta+}$, $O^{\delta-}$). When the promoting species does not react appreciably with any of the reactants (e.g., $Na^{\delta+}$), then P_i can be measured easily. P_i values up to 250 have been measured (41). When the promoting species is also partially consumed by one of the reactants, as in the case of C_2H_4 oxidation when YSZ is used as the solid electrolyte support (in which case, as analyzed below, C_2H_4 reacts with the promoting species $O^{\delta-}$ at a rate Λ times smaller than that with normally chemisorbed oxygen), then the measurement of P_i is more complicated due to the difficulties in measuring the surface coverage of $O^{\delta-}$. In such cases a conservative estimate of P_i can be obtained from $P_i = (\Delta r/r_0)_{max}$, i.e., by assuming that the maximum rate enhancement is obtained for $\Delta\theta_{O^{\delta-}} = 1$ (45).

The NEMCA effect can be explained by taking into account the effect of the potentiostatically or galvanostatically controlled back-spillover of promoting species from the solid electrolyte onto the gas-exposed catalyst surface and the effect of these species on the binding strength of chemisorbed reactants and intermediates (21).

The main conclusion which has emerged from previous NEMCA studies (20–44) is that over wide ranges of catalyst work function $e\Phi$ (0.1–1.0 eV), which can be controlled easily by potenstiostatically controlling the coverage of the promoting species on the catalyst surface (20), catalytic rates, r, depend exponentially on $e\Phi$,

$$\ln(r/r_0) = \alpha(e\Phi - e\Phi^*)/k_bT, \qquad [3]$$

where r_0 is the open-circuit (unpromoted) catalytic rate and α and $e\Phi^*$ are reaction-specific and catalyst-specific constants. The parameter α (positive for electrophobic reactions, negative for electrophilic ones) usually takes values between -1 and 1.

The present work is the first detailed study of NEMCA on Rh. The oxidation of C_2H_4 was chosen as a model reaction. The reaction is known to exhibit a pronounced electrophobic NEMCA effect on Pt (24) and on Ag (33). It is found that NEMCA induces very pronounced (up to one hundredfold) increases in catalytic rate. The measured rate enhancement ratio $\rho(r/r_0)$ values are the highest measured so far in *in situ* controlled promotional (NEMCA) studies.

EXPERIMENTAL

The apparatus utilizing on-line gas chromatography (Perkin–Elmer, Sigma 300B), mass spectrometry (Balzers QMG 311), and IR spectroscopy (Beckman 864 CO_2 analyzer) has been described previously (21–25).

Reactants were Messer Griesheim certified standards of C_2H_4 in He and O_2 in He. They could be further diluted in ultrapure (99.999%) He (L'Air Liquide).

The atmospheric pressure YSZ continuous-flow reactor shown schematically in Fig. 1 has been described previously (21–25). It has a volume of 30 cm^3 and behaves as a CSTR in the flow range of 50–300 cm^3 STP/min, as shown previously by determination of its residence time distribution using an IR CO_2 analyzer (21). The conversion of the reactants under open- or closed-circuit conditions was kept below 20%.

The porous Rh catalyst film was deposited on the inside bottom wall of the YSZ tube by application of a thin coating of Engelhard (Hanovia) A8826 Rh resinate, followed by drying and calcining in air, first at 400°C for 2 h and then at 850°C for 6 h. The thickness of the film was of order 10 μm, its superficial surface area was 2 cm^2, and its true surface was area 20 cm^2 (reactive oxygen

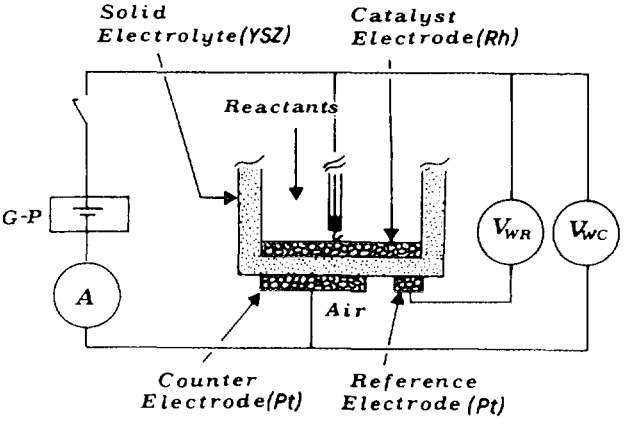

FIG. 1. Schematic of the bottom section of the YSZ tube reactor showing the location of the catalyst film and of the counter and reference electrodes.

uptake $N = 3.6 \times 10^{-8}$ g-atom O) determined by the isothermal titration technique (21) using oxygen titration with CO at 350°C. Platinum counter and reference electrodes were deposited on the outer surface of the YSZ bottom wall (Fig. 1) using Engelhard Pt paste A-1121 followed by drying and calcination, first at 400°C for 2 h then at 850°C for 6 h, as described elsewhere (21).

In the course of the experimental programme both galvanostatic and potentiostatic operations were used, by means of an AMEL 553 galvanostat–potentiostat, and both gave similar results. In the galvanostatic mode a constant current I is applied between the catalyst and the counterelectrode while monitoring the ohmic-drop-free (21, 24) catalyst potential V_{WR} between the catalyst (working electrode, W) and the reference (R) electrode. To obtain V_{WR} one must subtract the parasitic working–reference $(IR)_{WR}$ ohmic drop from the measured V'_{WR} value. This was done via the current interruption technique, utilizing a memory oscilloscope (Hameg HM-205) as in previous NEMCA studies (21, 24). In the present work $(IR)_{WR}$ was found to be typically less than 50 mV. In the potentiostatic mode a constant potential V_{WR} is applied between the catalyst and the reference electrode while monitoring the current, I, between the catalyst and the counter electrode. Changes in the catalyst potential, V_{WR}, are related to concomitant changes in catalyst work function, $e\Phi$, via

$$e\Delta V_{WR} = \Delta(e\Phi), \qquad [4]$$

as predicted theoretically (21) and established experimentally by *in situ* measurement of $e\Phi$ with a Kelvin probe on Pt and Ag catalyst electrodes deposited on YSZ and β''-Al_2O_3 (20, 30).

RESULTS

Open-Circuit Kinetics

Figure 2 shows the effect of oxygen partial pressure P_{O_2} on the rate, r, of C_2H_4 oxidation and on the open-circuit catalyst potential V^0_{WR} at constant $P_{C_2H_4}$. The rate first increases with P_{O_2} and then, at a critical P_{O_2} value, hereafter denoted by $P^*_{O_2}$, decreases abruptly and becomes negative-order in oxygen. The abrupt rate decrease is accompanied by an abrupt increase in the open-circuit catalyst potential V^0_{WR} and thus (20, 30) in work function $e\Phi$.

The rate, V^0_{WR}, and $e\Phi$ dependence on $P_{C_2H_4}$ at constant P_{O_2} is shown in Fig. 3. The rate is near first-order in ethylene until a critical $P_{C_2H_4}$ value is reached, hereafter denoted by $P^*_{C_2H_4}$, at which the rate increases abruptly to a much higher value. This is accompanied by an abrupt decrease in V^0_{WR} and $e\Phi$. Upon further increase in $P_{C_2H_4}$ above $P^*_{C_2H_4}$ the rate remains positive-order in ethylene. Increasing temperature causes an increase in $P^*_{O_2}$ and a decrease in $P^*_{C_2H_4}$.

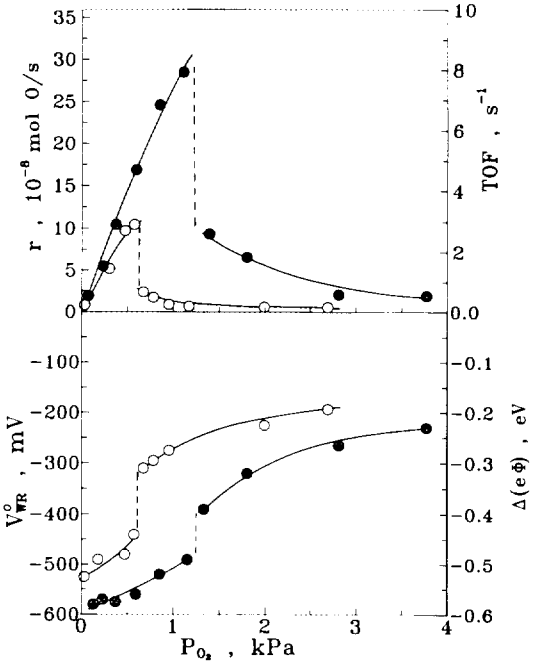

FIG. 2. Effect of oxygen partial pressure on the open-circuit catalytic rate (upper) and on the open-circuit catalyst potential V^0_{WR} and work function change (lower). Conditions: T = 320°C, $P_{C_2H_4}$ = 3 kPa (open circles); T = 350°C, $P_{C_2H_4}$ = 5 kPa (filled circles).

The kinetic behaviour depicted in Figs. 2 and 3 provides strong evidence that the abrupt rate transition is due to the formation of a surface Rh oxide (1, 15, 16). This is because if the sharp r vs P_{O_2} maximum (Fig. 2) were due to competitive adsorption of oxygen and ethylene, this would also show up as a rate maximum in the r vs $P_{C_2H_4}$ plots (Fig. 3), which is clearly not the case.

From a thermodynamic viewpoint, formation of an oxide is expected to occur at constant open-circuit catalyst potential, V^0_{WR}, and thus constant surface oxygen activity, a_O, which can be computed from V^0_{WR} via (21, 46, 47)

$$V^0_{WR} = (RT/4F)\ln[a_O^2/(0.21)], \qquad [5]$$

where 0.21 is the oxygen activity at the reference Pt/air electrode. Equation [5] is valid only under open-circuit conditions, and only provided that the dominant potential-setting charge-transfer reaction at the three-phase-boundary (tpb) metal–YSZ–gas is

$$O^{2-}(YSZ) \rightleftharpoons O(a) + 2e^-, \qquad [6]$$

where $O(a)$ designates oxygen adsorbed on the metal electrodes at the tpb. Figures 2 and 3 show that surface Rh

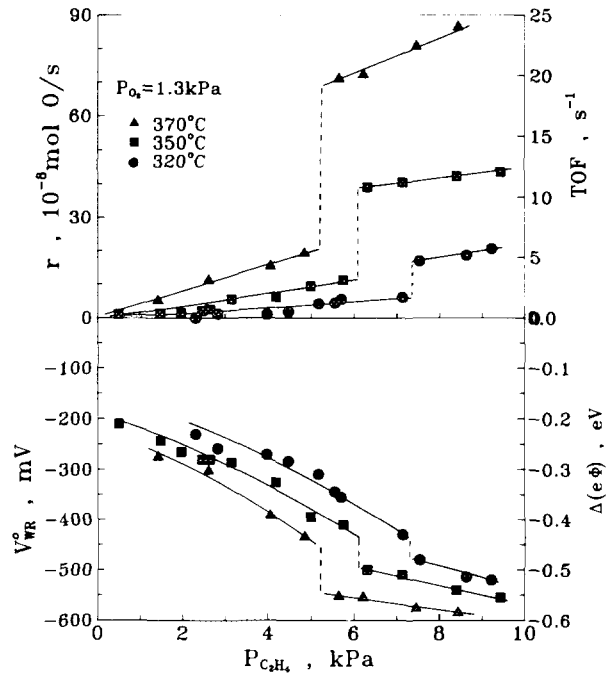

FIG. 3. Effect of ethylene partial pressure on the open-circuit catalytic rate (upper) and on the open-circuit catalyst potential V^0_{WR} and work function change (lower). P_{O_2} = 1.3 kPa.

oxide formation is accompanied by a significant, up to 150 mV, shift in V^0_{WR}. This is due to the significantly higher catalytic activity of the reduced surface ($P_{O_2} < P^*_{O_2}$, $P_{C_2H_4} > P^*_{C_2H_4}$) as compared to the oxidized surface, which can lead to such abrupt oxygen activity variations near the surface oxide stability limit, as analysed by Riekert (48) and as observed experimentally in previous studies of C_2H_4 (46) and CO (47) oxidation on Pt.

Figure 4 shows the upper limit (oxidized surface) of catalyst potential and corresponding oxygen activity, a_O, at which the abrupt rate transition takes place. The fact that $\ln a_O^2$ increases linearly with T^{-1} with a slope corresponding to ΔH = 21 kcal/mol O, i.e., comparable to the value for bulk Rh oxides (Fig. 4), further corroborates the assignment of this rate transition to surface oxide formation and the assignment of a_O^2 at which the transition takes place to the stability limit of surface Rh oxide. The formation of several Rh oxide phases on Rh is well documented both in atmospheric pressure studies (15, 16) and under UHV conditions (1).

NEMCA Behaviour: Transients and the Physical Meaning of Λ

Figure 5a shows a typical NEMCA galvanostatic transient; i.e., it depicts the response of the rate of C_2H_4 oxidation on Rh upon imposition of a constant current I. Under such conditions O^{2-} is transferred from the solid electrolyte to the catalyst at a rate $I/2F$ while at the same time O_2 (g) is reduced to O^{2-} at the counterelectrode at the same rate. Throughout the experiment the inlet P_{O_2} and $P_{C_2H_4}$ values are 2.6 kPa and 5.9 kPa and the volumetric flowrate is 175 cm^3 STP/min.

At the beginning of the experiment ($t < 0$), no current is applied ($I = 0$), and the open-circuit catalytic rate is 1.8×10^{-8} (mol O/s), corresponding to an oxygen conversion of 0.3%. Then at $t = 0$ a constant current I = 400 μA is applied via the galvanostat and O^{2-} is transferred to the catalyst at a rate $I/2F = 2.07 \times 10^{-9}$ mol O/s. This causes an 88-fold (8800%) increase in catalytic rate, which stabilizes to a new value $r = 1.62 \times 10^{-6}$ (mol O/s).

The rate increase $\Delta r = 1.60 \times 10^{-6}$ mol O/s is 770 times larger than the rate of O^{2-} supply $I/2F$. Thus each O^{2-} ion supplied to the catalyst causes, on the average, 770 chemisorbed O atoms to react with C_2H_4 and form CO_2 and H_2O.

The NEMCA time constant τ is defined (21, 24) as the time required for the rate increase to reach 63% of its steady-state value during a galvanostatic transient. In the present case τ is found to be 40 s, in good qualitative agreement with the parameter $2FN/I$ = 18 s, where $N = 3.6 \times 10^{-8}$ mol O is the reactive oxygen catalyst uptake, measured via surface titration with CO (21). This qualitative agreement is typical of NEMCA studies utilizing YSZ and corroborates the well-established proposition that the NEMCA effect is due to the electrochemically induced and controlled back-spillover of O^{2-} onto the catalyst surface and that these back-spillover oxide ions act as promoters for the catalytic reaction.

It is worth noting that when steady-state has been reached during a galvanostatic transient, the rate, $r_{O^{2-}}$, of consumption of the back-spillover oxide ions on the cata-

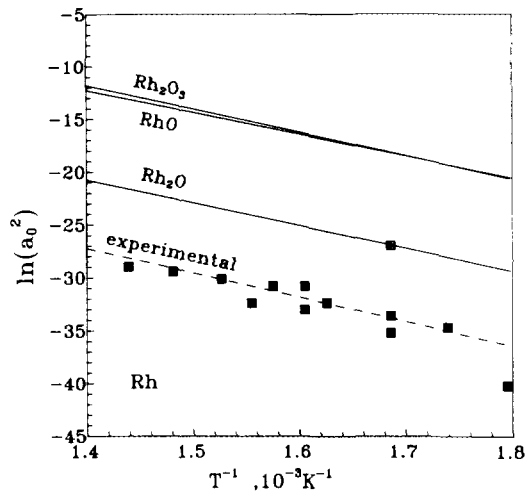

FIG. 4. Temperature effect on the surface oxygen activity of the oxidized surface at the rate transition ($P_{O_2} = P^*_{O_2}$, $P_{C_2H_4} = P^*_{C_2H_4}$) and comparison with the stability limits of bulk Rh oxides.

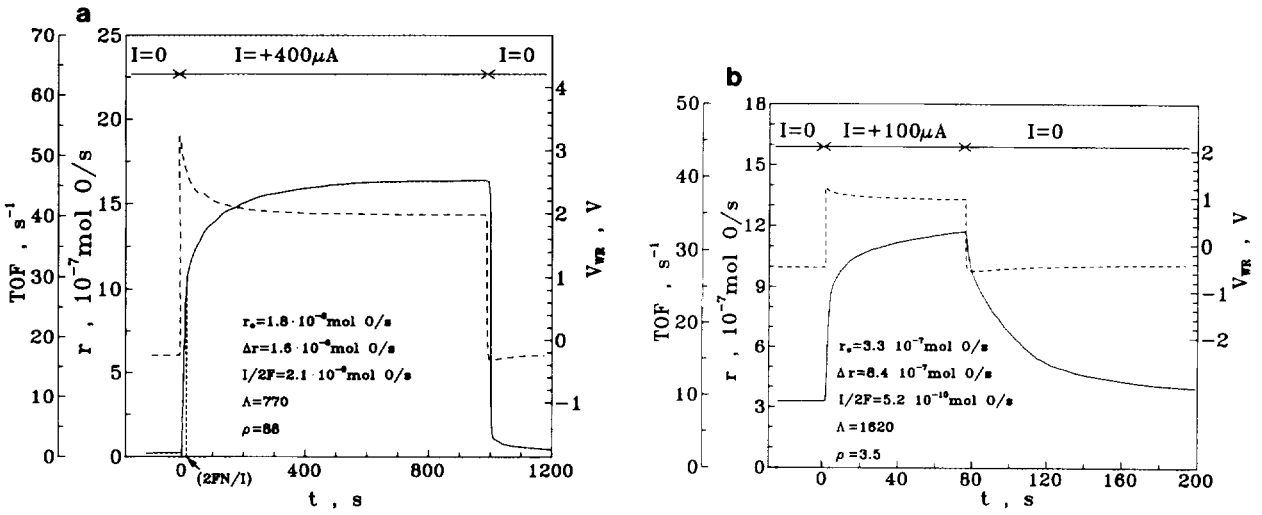

FIG. 5. Rate (solid line) and catalyst potential (dotted line) response to a step change in applied current. Conditions: (a) T = 350°C; inlet P_{O_2} and $P_{C_2H_4}$ values, $P^0_{O_2}$ = 2.6 kPa and $P^0_{C_2H_4}$ = 5.9 kPa; (b) T = 350°C, P_{O_2} = 2.1 kPa, $P_{C_2H_4}$ = 8.8 kPa.

lyst surface must equal their rate of supply $I/2F$,

$$r_{O^{2-}} = I/2F. \quad [7]$$

The enhancement factor or Faradaic efficiency, Λ, is defined by

$$\Lambda = \Delta r/(I/2F), \quad [1a]$$

where $\Delta r = r - r_0$, with r and r_0 being the NEMCA-induced and open-circuit catalytic rates, respectively. To the extent that $r \gg r_0$, i.e., $\Lambda \gg 1$, as in the present case, one can write

$$\Lambda \approx r/(I/2F), \quad [8]$$

and thus from Eq. [1a]

$$\Lambda \approx r/r_{O^{2-}}. \quad [9]$$

Consequently Λ expresses the ratio of the reaction rates of normally chemisorbed atomic oxygen and of back-spillover oxide ions with C_2H_4. It follows, therefore, that the spillover oxide ions are significantly less reactive than normally chemisorbed oxygen, in agreement with the results of the XPS investigation of NEMCA on Pt/YSZ under UHV conditions (45). This is further corroborated by the transient rate behaviour upon current interruption, e.g., Fig. 5a. As shown in this figure, it takes approximately 20 s in this case for the catalytic rate to reach its open-circuit (unpromoted) value, i.e., for O^{2-} to be consumed by C_2H_4. This value can be predicted from the steady-state results of Fig. 5a via Eq. [7] or Eq. [9] as follows. At the steady state of the galvanostatic transient it is (Eq. [7] or [9]) $r_{O^{2-}} = 2.07 \times 10^{-9}$ mol/s. Taking into account that the reactive oxygen uptake of the catalyst is $N = 3.6 \times 10^{-8}$ mol/s and assuming that the O^{2-} coverage value, $\theta_{O^{2-}}$, before current interruption is unity (45), it follows that the average lifetime, $\tau_{O^{2-}}$ of O^{2-} on the catalyst surface is

$$\tau_{O^{2-}} = N\theta_{O^{2-}}/r_{O^{2-}} = 18 \text{ s}, \quad [10]$$

which is in excellent agreement with the experimental value of 20 s (Fig. 5a). A detailed analysis of rate transients upon current interruption will appear elsewhere (50).

The operating conditions in Fig. 6a were chosen so that the surface is initially ($t < 0$) in the oxidized state, whereas in the final steady state condition ($t > 0$) the surface is in a reduced state. This is at first surprising, since application of a positive current or potential would be expected to stabilize the surface Rh oxide. However, as shown in detail below, increasing catalyst potential weakens the chemisorptive bond of atomic oxygen, in agreement with previous NEMCA studies and theoretical considerations (21), and thus facilitates the oxide reduction, as manifested both by the observed dramatic rate enhancement and by the sharp and peculiar V_{WR} vs t response (Fig. 5a).

Figure 5b shows another galvanostatic transient. In this case the operating $P_{C_2H_4}$ and P_{O_2} were chosen such that the surface is initially ($t < 0$) reduced. In this case the observed rate enhancement ratio ρ ($=r/r_0$) is significantly smaller (3.5), the Faradaic efficiency Λ value (1620) is high and the V_{WR} vs t maximum is less pronounced.

It should be noted that the order of magnitude of the measured Λ values is in good agreement with the parame-

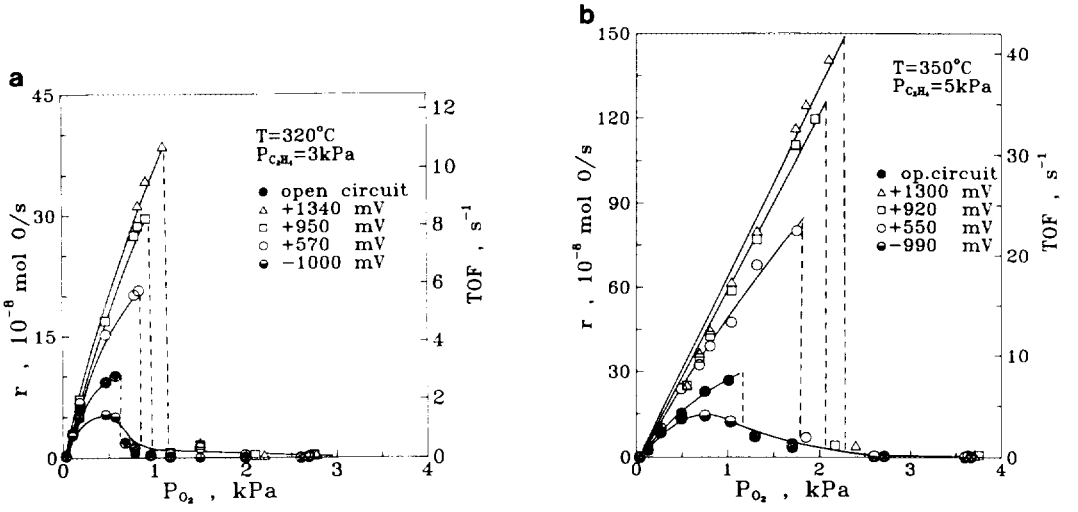

FIG. 6. Effect of P_{O_2} and imposed catalyst potential V_{WR} on the rate of C_2H_4 oxidation. (a) T = 320°C, $P_{C_2H_4}$ = 3 kPa. (b) T = 350°C, $P_{C_2H_4}$ = 5 kPa.

ter $2Fr_0/I_0$ as in previous NEMCA studies (21). This is shown in Tables 1 and 2. Table 1 presents the measured values of the exchange current I_0, extracted from current–overpotential plots under reaction conditions (21). It is worth noting that I_0 is higher on the reduced surface than on the oxidized surface.

Steady-State Effect of Catalyst Potential

Figures 6a and 6b show the effect of P_{O_2} and catalyst potential on the rate and turnover frequency (TOF) of C_2H_4 oxidation for two different fixed values of $P_{C_2H_4}$ and at various fixed imposed values of catalyst potential V_{WR}. The r vs P_{O_2} behaviour is also depicted for open-circuit, i.e., normal catalytic, conditions (I = 0, V_{WR} = V^0_{WR}). The open-circuit V^0_{WR} varies between −500 and −100 mV as P_{O_2} varies between 0.1 and 3 kPa.

For low P_{O_2} values (reduced surface, $P_{O_2} < P^*_{O_2}$) increasing V_{WR} causes a significant, up to threefold, increase in the reaction rate relative to its open-circuit value. The main feature, however, is the significant increase in $P^*_{O_2}$ with increasing V_{WR}, which causes a dramatic, up to a hundredfold, increase in catalytic rate for intermediate P_{O_2} values. For higher P_{O_2} values there is practically no effect.

It is remarkable that increasing V_{WR}, which corresponds to positive currents, i.e., to O^{2-} supply to the catalyst, increases $P^*_{O_2}$, i.e., destabilizes the surface Rh oxide. This is due to the weakening of the Rh=O bond, but also strengthening of the Rh-C_2H_4 chemisorptive bond, with increasing V_{WR} and work function $e\Phi$ according to the theory of electrochemical promotion (21).

Figures 7a and 7b, obtained at 320 and 350°C, respectively, show the effect of $P_{C_2H_4}$ and fixed catalyst potential V_{WR} on the rate of C_2H_4 oxidation. The figures also compare the rate with that measured under open-circuit (o.c.) conditions where again V^0_{WR} varies between −50 and −500 mV as $P_{C_2H_4}$ varies between 0.1 and 10 kPa.

The low rate branch of Figs. 7a and 7b corresponds to an oxidized surface ($P_{C_2H_4} < P^*_{C_2H_4}$). On this surface the rate is first-order in ethylene and is practically unaffected by V_{WR}. The high rate branch of Figs. 7a and 7b corresponds to a reduced surface. The main feature of these figures is the significant shift in $P^*_{C_2H_4}$ with varying V_{WR}. It is remarkable that $P^*_{C_2H_4}$ shifts from 2 kPa for V_{WR} = 1340 mV to a value above 10 kPa for V_{WR} = −1000 mV. In the latter case the Rh=O bond is so strong and the Rh-ethylene bond so weak, that even high (>10 kPa) $P_{C_2H_4}$ cannot reduce the surface. As a result of the ob-

TABLE 1

Exchange Current I_0/μA for $P_{O_2} \approx$ 5 kPa and $P_{C_2H_4} \approx$ 2.5 kPa

T (°C)	320	350	370
Oxidized surface	13	22	—
Reduced surface	—	72	90

TABLE 2

Predicted ($2Fr_0/I_0$) and Measured Λ Values

	$2Fr_0/I_0$	Λ
Fig. 5a	160	770
Fig. 5b	2270	1620

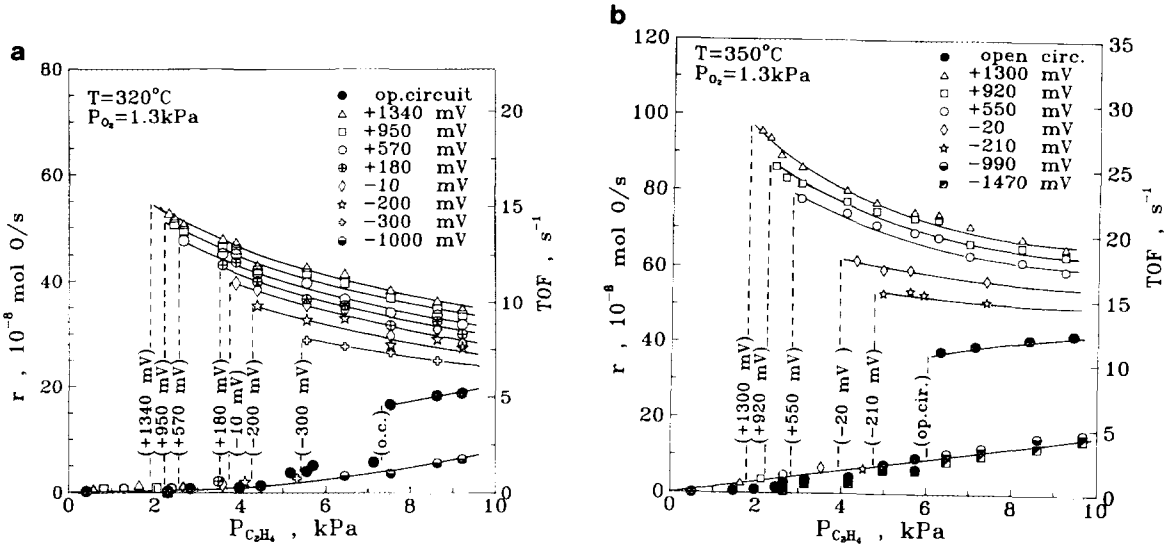

FIG. 7. Effect of $P_{C_2H_4}$ and imposed catalyst potential V_{WR} on the rate of C_2H_4 oxidation. P_{O_2} = 1.3 kPa. (a) T = 320°C, (b) T = 350°C.

served pronounced decrease in $P^*_{C_2H_4}$ with increasing V_{WR}, the rate enhancement ratio $\rho(= r/r_0)$ is up to 100 for V_{WR} = 1340 mV.

Another important feature of Figs. 7a and 7b is the change in the reaction order with respect to ethylene on the reduced surface. Thus, under open-circuit conditions, the rate remains positive-order in ethylene on the reduced surface. Under imposed positive-overpotential (and current) conditions, however, the rate on the reduced surface becomes negative-order with respect to ethylene. This strongly suggests competitive chemisorption of ethylene and of the back-spillover oxide ions on the Rh surface. It is worth emphasizing that XPS investigation of NEMCA on Pt has shown that the coverage of the back-spillover oxide ions can be as high as that of normally chemisorbed oxygen for V_{WR} values of 1200 mV and that the two species coexist on the surface at high coverages, presumably bonded on different surface sites (45).

It is worth noticing again that the main feature of Figs. 6 and 7 is the pronounced destabilization of surface Rh oxide with increasing catalyst potential, which is the main cause of the observed dramatic rate enhancement.

Figures 8a and 8b show in detail the effect of catalyst potential V_{WR} and the corresponding rate of O^{2-} supply $I/2F$ on the rate of C_2H_4 oxidation at fixed gaseous composition.

The first gaseous composition (Fig. 8a) was chosen so that the surface is reduced and remains reduced with positive and negative current application. The reaction exhibits electrophobic (i.e., $\Lambda > 1$) behaviour with Λ values as high as 15,000 for both positive and negative currents. The rate variation is moderate as r/r_0 varies between 0.25 and 2.

It is also worth noting that:

1. The r/r_0 vs V_{WR} curves exhibit a rather narrow region of exponential dependence for -1 V $< V_{WR} < -0.5$ V,

$$\ln(r/r_0) = \alpha e \Delta V_{WR}/k_b T, \qquad [11]$$

with an α value of 0.2.

2. The rate variation with V_{WR} diminishes with increasing T so that for T = 370°C, V_{WR} has practically no effect on the rate for $V_{WR} > -1$ V. This is directly related to the appearance of the compensation effect with an isokinetic point at 372°C as discussed below.

The gaseous compositions in Fig. 8b were chosen such that the open-circuit conditions correspond to an oxidized surface ($P_{O_2} > P^*_{O_2}$, $P_{C_2H_4} < P^*_{C_2H_4}$). At low temperatures ($T$ = 320°C) the surface remains oxidized over the entire V_{WR} range and thus the measured ρ and Λ values are moderate. At higher temperatures, positive currents and potentials lead to a reduction in surface oxide and the rate enhancement is very pronounced. Thus, as shown in Fig. 8b, Λ values up to 50,000 and $\rho(=r/r_0)$ values up to 100 are obtained.

The observed steady-state multiplicity with respect to V_{WR} (Fig. 8b) is due to the oxide decomposition in conjunction with the galvanostatic operation. Potentiostatic operation leads to steady-state multiplicity with respect to the current.

Effect of V_{WR} and Work Function on Activation Energy: Compensation Effect

Figure 9 shows Arrhenius plots obtained at fixed V_{WR} values. The gas composition is reducing so that all points

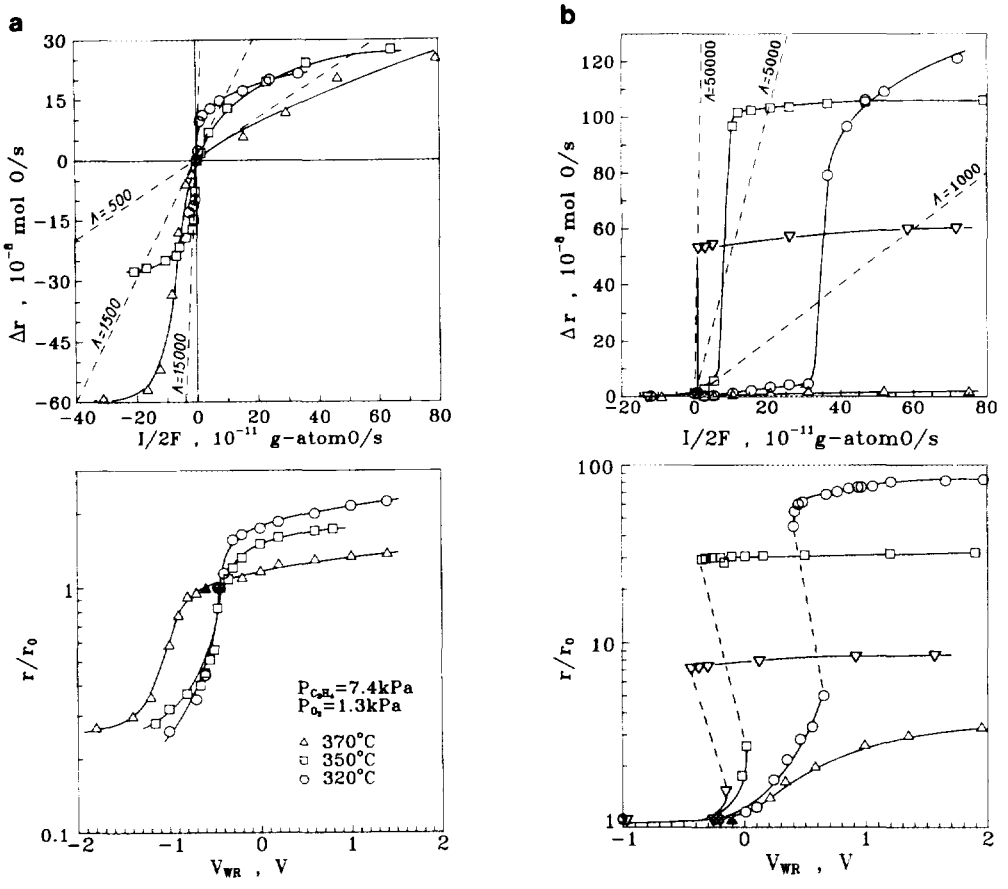

FIG. 8. Effect of applied current (upper) and corresponding catalyst potential V_{WR} (lower) on the rate of C_2H_4 oxidation on a Rh surface which is reduced (a) or oxidized (b) under open-circuit conditions. Filled symbols correspond to open-circuit conditions, i.e., to the unpromoted catalyst. Conditions: (a) P_{O_2} = 1.3 kPa, $P_{C_2H_4}$ = 7.4 kPa, r_0 = 1.74 × 10^{-7} mol/s (○), 6.5 × 10^{-7} mol/s (□), 8.4 × 10^{-7} mol/s (△); (b) P_{O_2} = 5 kPa, $P_{C_2H_4}$ = 2.5 kPa; (△) T = 320°C, r_0 = 0.87 × 10^{-8} mol/s; (○) T = 350°C, r_0 = 1.8 × 10^{-8} mol/s; (□) T = 370°C, r_0 = 3.67 × 10^{-8} mol/s; (▽) P_{O_2} = 1.2 kPa, $P_{C_2H_4}$ = 3 kPa, T = 350°C, r_0 = 9.6 × 10^{-8} mol/s.

in Fig. 9 correspond to a reduced surface. The open-circuit V^0_{WR} is −500 to −600 mV. Increasing V_{WR} causes a dramatic decrease in activation energy from 0.92 eV (open-circuit conditions) to 0.3 eV for V_{WR} = 0.8 V and a concomitant pronounced decrease in the preexponential factor, r^0, defined from

$$r = r^0 \exp(-E/k_bT). \qquad [12]$$

As a result of this, Fig. 9 presents a striking demonstration of the compensation effect (51–53) with an isokinetic point at T_Θ = 372°C. The compensation effect in heterogeneous catalysis has been the focal point of numerous studies and debates (51–53). It is usually obtained from Arrhenius plots of several similar reactions on the same catalyst or of several similar catalysts for the same reaction. In the present case it is obtained for one reaction and one catalyst by varying its potential or, equivalently, by varying the level of the promoting species (O^{2-}) on its surface. Since the isokinetic point is usually outside the temperature range of the kinetic investigation, several authors have even questioned the existence of a true compensation effect (53). Consequently the results in Fig. 9, where the isokinetic point T_Θ lies within the investigated temperature range, are rather rare and provide direct evidence that the compensation effect is a real one. Similar compensation effect plots have been recently obtained in electrochemical promotion (NEMCA) studies of other catalytic reactions and a review is given elsewhere (50).

It is worth noting in Fig. 9 that below the isokinetic point ($T < T_\Theta$) the reaction exhibits electrophobic behaviour (21), i.e., $\partial r/\partial V_{WR} > 0$ and thus $\alpha > 0$ and $\Lambda > 0$, while above the isokinetic point ($T > T_\Theta$) the reaction exhibits electrophilic behaviour (21), i.e., $\partial r/\partial V_{WR} < 0$ and thus $\alpha < 0$ and $\Lambda < 0$. At $T = T_\Theta$ the NEMCA effect disappears (compare also the curve for T = 370°C in Fig. 8a).

As shown in Fig. 10 the decrease in activation energy with eV_{WR} and $e\Phi$ is nearly linear, with a slope of −0.5. Also the logarithm of the preexponential factor r^0 de-

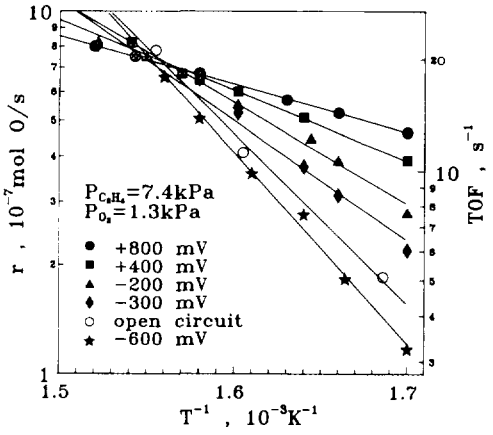

FIG. 9. NEMCA-induced compensation effect. Arrhenius plots at fixed V_{WR} values. P_{O_2} = 1.3 kPa, $P_{C_2H_4}$ = 7.4 kPa.

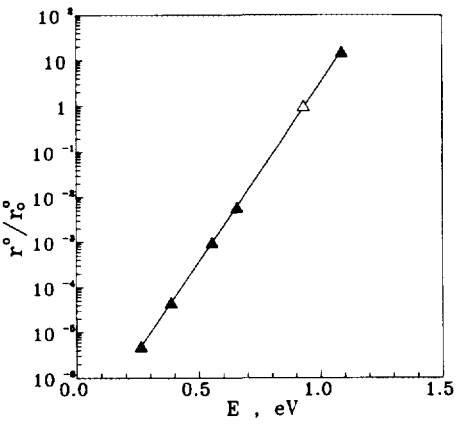

FIG. 11. Dependence of the preexponential factor r^0 on the activation energy E. r_0^0 = 16.54 mol O/s. Open symbol corresponds to open circuit. Conditions are as in Fig. 9.

creases linearly with V_{WR} (Fig. 10) and upon plotting $k_b T_\Theta \ln(r^0/r_0^0)$, where r_0^0 is the open-circuit preexponential factor, vs eV_{WR} the slope is again −0.5 (Fig. 10). In fact the difference between the two parallel lines equals the open-circuit activation energy E_0 as shown in Discussion and as observed experimentally (Fig. 10).

Figure 11 shows that, as a result of Figs. 9 and 10, the logarithm of the preexponential factor r^0 increases linearly with E with a slope of 18 eV^{-1}.

DISCUSSION

The present results establish that the catalytic properties of Rh can be markedly affected via the NEMCA effect by using Y_2O_3-stabilized ZrO_2 (YSZ) as an active catalyst

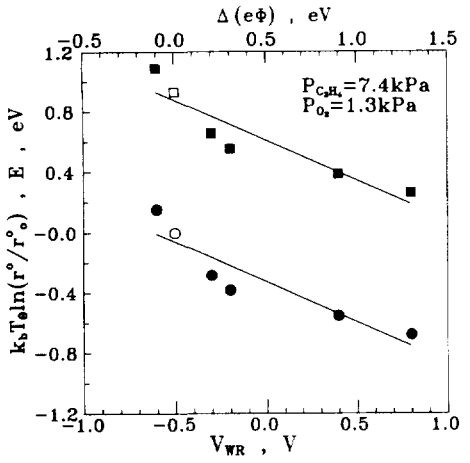

FIG. 10. Effect of catalyst potential V_{WR} and corresponding work function change $\Delta(e\Phi)$ on the activation energy (squares) and preexponential factor r^0 (circles). Open symbols correspond to open circuit. r_0^0(=16.54 mol O/s) is the open-circuit preexponential factor and T_Θ is the isokinetic temperature. Conditions are the same as in Fig. 9.

support and promoter donor. The maximum observed catalytic rate enhancement ($\rho = r/r_0 \approx 100$) is the highest reported so far in NEMCA studies (20–44). The measured Faradaic efficiency, Λ, values are typically on the order of 10^4, in good qualitative agreement with

$$|\Lambda| \approx 2Fr_0/I_0, \quad [13]$$

according to the theory of NEMCA (21). The same applies for the relaxation time constant τ during galvanostatic transients which conform to

$$\tau \approx 2FN/I. \quad [14]$$

Thus, similar to the case of Pt and Ag interfaced with YSZ (21), the effect must be due to the promoting action of back-spillover oxide ions $O^{\delta-}$ which migrate onto the catalyst surface from the YSZ solid electrolyte under the influence of the applied potential. The back-spillover oxide ions spread on the catalyst surface, increase its work function $e\Phi$ by (20, 21, 30)

$$\Delta(e\Phi) = e\Delta V_{WR}, \quad [4]$$

and act as promoters by affecting the binding strength of covalently bonded adsorbates such as normally chemisorbed oxygen and ethylene. The migration of the back-spillover oxide ions from the YSZ onto the metal surface under the influence of the applied potential has been positively confirmed by *in situ* XPS for the cases of Pt (45, 49) and Ag (54) catalysts. The O 1*s* binding energy of the back-spillover oxide ions is approximately 529 eV (45).

The coverage of back-spillover oxide ions can be as high as that of normally chemisorbed oxygen for high (~1 V) applied potentials. Consequently, an approximate estimate of the promotion index P_i(41) of the oxide ions for C_2H_4 oxidation can be obtained as follows. Assuming

that the maximum observed rate enhancement, r/r_0 ($\approx$100), corresponds to the maximum coverage of $O^{\delta-}$ (roughly equal (45) to the maximum coverage of normally chemisorbed oxygen taken as unity), it follows that $P_i = \Delta(r/r_0)/\Delta\theta_{O^{2-}} \approx 100$.

It should be emphasized that, as analyzed under Results, and as evidenced by XPS (45), the back-spillover oxide ions can act as promoters because they are Λ ($\sim 10^4$) times less reactive with C_2H_4 than normally chemisorbed oxygen.

Origin of the Promoting Action

The open-circuit kinetic and V^0_{WR} behaviour (Figs. 2 and 3) show clearly the existence of two kinetic regimes corresponding to an oxidized and a reduced surface, respectively. The catalytic rate on the reduced surface is much higher than on the oxidized surface. The transition from a reduced surface to an oxidized surface occurs at a certain temperature-dependent and $P_{C_2H_4}$-dependent oxygen pressure values $P^*_{O_2}$ or at a certain temperature-dependent and P_{O_2}-dependent values of ethylene pressure $P^*_{C_2H_4}$. The potentiometrically determined oxygen activity values a_O provides strong evidence that the transition is due to the formation of surface Rh oxide with a ΔH of $\sim$20 kcal/mol O or $\sim$40 kcal/mol O_2 (Fig. 5).

On the reduced surface the rate is first-order in oxygen and positive-order in ethylene. The activation energy is near 1 eV. The reaction between chemisorbed atomic oxygen and ethylene appears to be rate controlling (Figs. 2 and 3). There is no evidence for competitive adsorption.

On the oxidized surface, the rate is first-order in ethylene and negative-order in oxygen. This indicates competitive adsorption and a predominantly oxygen-covered surface.

The same general kinetic features are observed under closed-circuit, i.e., NEMCA, conditions (Figs. 6 and 7) with three notable differences:

I. The $P^*_{O_2}$ and $P^*_{C_2H_4}$ values shift significantly with varying potential. This causes a dramatic (up to 100-fold) enhancement in catalytic rate for intermediate P_{O_2} and $P_{C_2H_4}$ values.

II. Increasing V_{WR} also causes a significant rate increase on the reduced surface but has practically no effect on the oxidized surface.

III. On the reduced surface the rate becomes negative-order in ethylene, which indicates competitive adsorption of back-spillover oxide ions and ethylene.

The above observations show that, despite the observed dramatic rate enhancement, the mechanism of C_2H_4 oxidation remains the same under both open-circuit and closed-circuit conditions, i.e., NEMCA and the back-spillover oxide ion promoters do not create new reaction pathways but simply accelerate existing ones.

Consequently, in order to rationalize the observed pronounced promotional phenomena one must examine the effect of the presence of the back-spillover oxide ions and concomitant change in catalyst potential V_{WR} and work function $e\Phi$ on the binding strength of dissociatively chemisorbed oxygen and chemisorbed ethylene.

All previous electrochemical promotion (NEMCA) results in catalysis (20–44) have been rationalized in terms of the following simple and theoretically well-established rule (21). Increasing the V_{WR} and $e\Phi$ of the catalyst surface by supplying back-spillover negatively charged ions ($O^{\delta-}$, F^-) causes a weakening in the chemisorptive bond strength of electron acceptor adsorbates, such as dissociatively chemisorbed oxygen, and a strengthening in the chemisorptive bond strength of electron donor adsorbates such as ethylene. Exactly the opposite trends hold upon decreasing V_{WR} and $e\Phi$ of the catalyst surface via supply of positively charged ions, e.g., $Na^{\delta+}$ (20, 21).

The present results are in excellent agreement with the above rule. Since atomic oxygen and ethylene behave as electron acceptor and electron donor, respectively, it follows that increasing V_{WR} causes a weakening in the Rh=O bond and a stregthening in the Rh-C_2H_4 bond, in excellent agreement with the observed effect of V_{WR} on $P^*_{O_2}$ and $P^*_{C_2H_4}$ (Figs. 6 and 7). Since increasing V_{WR} destabilizes the Rh=O bond, due to the increasing coverage of back-spillover oxide ions which exert repulsive through-the-metal or through-the-vacuum lateral interactions with chemisorbed oxygen, it follows that higher P_{O_2} values ($P^*_{O_2}$) are required to form surface Rh oxide (Figs. 6a and 6b).

Conversely, since increasing V_{WR} and coverage of back-spillover oxide ions stabilizes the Rh-C_2H_4 bond via enhanced π electron donation to the metal, it follows that smaller $P_{C_2H_4}$ values ($P^*_{C_2H_4}$) are required to reduce the surface Rh oxide, as experimentally observed (Figs. 7a and 7b).

The observed effect of V_{WR} on $P^*_{O_2}$ and $P^*_{C_2H_4}$ is at first glance counterintuitive since the surface Rh oxide is destabilized by supplying O^{2-} from the solid electrolyte *to* the catalyst surface. Alternatively, if one were to attempt to relate V_{WR} and oxygen activity, a_O, by using the Nernst equation for closed-circuit conditions, one would reach the conclusion that increasing oxygen activity destabilizes the surface Rh oxide. This simply demonstrates, however, how erroneous the use of the Nernst equation can be outside its realm of applicability, i.e., far from open-circuit conditions.

Compensation Effect

The fact that increasing V_{WR} weakens the Rh=O bond is further corroborated by the observed effect of V_{WR} on the activation energy E in the reduced state region (Fig.

10). Increasing eV_{WR} causes a near-linear decrease in E with a slope of -0.5 and a concomitant linear decrease in the log of the preexponential factor r^0. The decrease in E with increasing V_{WR} and $e\Phi$ is very similar to that observed with C_2H_4 oxidation on Pt (24) and can be rationalized on the basis of the effect of increasing $e\Phi$ (and backspillover oxide ion coverage) on the strength of the Rh=O bond, the cleavage of which is involved in the rate limiting step of C_2H_4 oxidation.

Increasing $e\Phi$ diminishes electron back-donation to chemisorbed oxygen and thus weakens the binding strength of the Rh=O bond by an amount $\Delta(\Delta H_0)$, where ΔH_0 is the enthalpy of adsorption of oxygen and, according to the Polanyi principle (55), decreases the activation energy of the oxidation reaction by $\Delta E = \Delta(\Delta H_0)$. An alternative but complementary point of view is that the Rh=O bond is destabilized upon increasing V_{WR} and $e\Phi$ due to the strong lateral repulsive interaction of chemisorbed oxygen and back-spillover oxide ions. Recent *ab initio* calculations of Pacchioni and one of us (56) have shown a linear decrease in the binding strength of oxygen chemisorbed on Cu (110) with increasing $e\Phi$ due to the coadsorption of negatively charged ions, in agreement with the trend observed in electrochemical promotion studies (21).

As shown in Fig. 10, the dependence of E and r^0 on work function change, $\Delta(e\Phi)$, can be described by

$$E = E_0 + \alpha_H \Delta(e\Phi) \quad [15]$$

$$k_b T_\Theta \ln(r^0/r_0^0) = \alpha_H \Delta(e\Phi), \quad [16]$$

where E_0 is the open-circuit activation energy (0.92 eV), $\alpha_H = -0.5$, and T_Θ is the isokinetic point ($T_\Theta = 372°C$). It follows from Eqs. [15] and [16] that

$$E - k_b T_\Theta \ln(r^0/r_0^0) = E_0, \quad [17]$$

as experimentally observed (Fig. 10). It should be noted that the existence of an isokinetic point follows directly from the experimental Eq. [17] or, in general, from the existence of a linear dependence between activation energy E and the logarithm of the preexponential factor r^0. This experimentally observed variation has been expressed in several previous NEMCA studies (20, 21, 24, 25, 33, 34) in the form of Eq. [15] plus

$$k_b T_0 \ln(r_0/r_0^0) = \alpha_S \Delta(e\Phi) \quad [18]$$

where T_0 is the mean temperature of the kinetic investigation, the subscript 0 always refers to open-circuit conditions ($\Delta(e\Phi) = 0$), and α_S is a catalyst-specific and reaction-specific constant satisfying approximately (20, 21, 24, 25, 33, 34) the equation

$$\alpha = \alpha_S - \alpha_H, \quad [19]$$

where α is the NEMCA coefficient in Eq. [3]. Here we show first that Eqs. [16] and [18] are equivalent and that either one, in conjunction with Eq. [15], guarantees the existence of an isokinetic point. Thus upon eliminating $\Delta(e\Phi)$ between Eqs. [15] and [18] one obtains

$$k_b T_0 \ln(r^0/r_0^0) = (\alpha_S/\alpha_H)(E - E_0). \quad [20]$$

Since in general (Eq. [12])

$$\ln(r/r^0) = -E/k_b T, \quad [21]$$

one obtains by combination with Eq. [20]

$$\ln(r/r_0^0) = -(\alpha_S/\alpha_H)E_0/k_b T_0 + [(\alpha_S/\alpha_H) - (T_0/T)](E/k_b T_0). \quad [22]$$

Equation [22] predicts the existence of an isokinetic temperature T_Θ, defined from

$$T_\Theta = T_0(\alpha_H/\alpha_S). \quad [23]$$

For $T = T_\Theta$ the last term in Eq. [22] vanishes and thus r equals a constant which is independent of E, $\ln r^0$ and thus of $\Delta(e\Phi)$.

One can then use Eq. [23] to eliminate T_0 and α_S from Eq. [18] and obtain Equation [16], the equivalent to Eq. [18], which contains the isokinetic temperature T_Θ instead of α_S.

Equation [23] can also be used to eliminate the term (α_S/α_H) from Eq. [22] to obtain

$$\ln(r/r_0^0) = -E_0/k_b T + (E/k_b)(T_\Theta^{-1} - T^{-1}), \quad [24]$$

which in combination with Eq. [15] gives

$$\ln r = \ln r_0^0 - E_0/k_b T + \frac{\alpha_H \Delta(e\Phi)}{k_b T}\left(\frac{T}{T_\Theta} - 1\right). \quad [25]$$

Noting that the first two terms on the right of Eq. [25] give the open-circuit (unpromoted) rate r_0, one obtains

$$\ln(r/r_0) = \frac{\alpha_H \Delta(e\Phi)}{k_b T}\left(\frac{T}{T_\Theta} - 1\right). \quad [26]$$

Upon comparing Eq. [26] with the general experimental equation [3] extracted experimentally in this and in previous NEMCA studies (20–44),

$$\ln(r/r_0) = \alpha \Delta(e\Phi)/k_b T, \quad [3]$$

it follows that the NEMCA coefficient α is given by

$$\alpha = \alpha_H \left(\frac{T}{T_\Theta} - 1 \right). \qquad [27]$$

Since in the present case $\alpha_H < 0$, it follows that for $T < T_\Theta$ it is $\alpha > 0$, i.e., the reaction exhibits electrophobic behaviour, and for $T > T_\Theta$ it exhibits electrophilic behaviour ($\alpha < 0$), in excellent agreement with experiment (Fig. 9). The decrease in α when $T < T_\Theta$ and T approaches T_Θ predicted by Eq. [27] is also in very good agreement with the experiments (Fig. 8). Note that for $T = T_\Theta$ it is $\alpha = 0$ and the NEMCA effect disappears (Figs. 8 and 9).

It is worth noting that by combining Eqs. [23] and [27] one obtains

$$\alpha = \alpha_S - \alpha_H + \left(\frac{T}{T_0} - 1 \right) \alpha_S. \qquad [28]$$

Consequently, the approximation $\alpha = \alpha_S - \alpha_H$ (Eq. [19]) holds well provided the temperature T for which α is computed does not differ much from the mean temperature T_0 of the kinetic investigation used to extract the α_S and α_H values, as observed experimentally (20, 21, 24, 25, 33, 34).

A review of the compensation effect in *in situ* controlled promotional studies is given elsewhere (50). From a fundamental viewpoint the origin of the compensation effect lies in the existence of a linear relationship between the enthalpy of activation $\Delta H^\#$ and the entropy of activation $\Delta S^\#$ of the rate limiting step of the catalytic reaction. The theoretical reason for the existence of this linear relationship is still a matter of study and debate (53). The present results, however, show that both $\Delta H^\#$ and $\Delta S^\#$ are linearly related to the catalyst work function.

In summary, the present study shows that the use of Y_2O_3-stabilized ZrO_2 as an active catalyst support to induce NEMCA leads to very pronounced and reversible alterations in the catalytic properties of Rh for ethylene oxidation. Back-spillover oxide ions act as promoters for this reaction. These oxide ions cannot form via gas-phase oxygen chemisorption (45). Solid electrolytes, in general, provide a unique way to control the state of metal catalyst surfaces precisely and *in situ* and to investigate the role of promoters in catalysis.

ACKNOWLEDGMENT

We thank the CEC JOULE, Human Capital and Mobility, and STRIDE programmes for financial support.

REFERENCES

1. Logan, A. D., Datye, A. K., and Houston, J. E., *Surf. Sci.* **245,** 280 (1991).
2. Hoogers, G., and King, D. A., *Surf. Sci.* **286,** 306 (1993).
3. Bowker, M., Guo, Q., and Joyner, R., *Surf. Sci.* **253,** 33 (1991); *Surf. Sci.* **257,** 33 (1991).
4. Kao, C.-T., Blackman, G. S., van Hove, M. A., and Somorjai, G. A., *Surf. Sci.* **224,** 77 (1989).
5. Bugyi, L., Kiss, J., Revesz, K., and Solymosi, F., *Surf. Sci.* **233,** 1 (1990).
6. Madenach, R. P., Abend, G., Mousa, M. S., Kreuzer, H. J., and Block, J. H., *Surf. Sci.* **266,** 56 (1992).
7. Gomelli, G., Dhanak, V. R., Paolucci, G., and Rosei, R., *Surf. Sci.* **260,** 1 (1992).
8. Schmatloch, V., and Kruse, N., *Surf. Sci.* **269/270,** 488 (1992).
9. Mate, C. M., Kao, C.-T., and Somorjai, G. A., *Surf. Sci.* **206,** 145 (1988).
10. Bowker, M., Guo, Q., and Joyner, R. W., *Surf. Sci.* **280,** 50 (1993).
11. Ren, D. M., and Liu, W., *Surf. Sci.* **232,** 316, 323 (1990).
12. Koster, A., and van Santen, R. A., *Surf. Sci.* **233,** 366 (1990).
13. Slavin, A. J., Bent, B. E., Kao, C.-T., and Somorjai, G. A., *Surf. Sci.* **206,** 124 (1988).
14. Levis, R. J., DeLouise, L. A., White, E. J., and Winograd, N., *Surf. Sci.* **230,** 35 (1990).
15. Kellogg, G. L., *Surf. Sci.* **171,** 359 (1986); *J. Catal.* **92,** 167 (1985).
16. Oh, S. H., and Carpenter, J. E., *J. Catal.* **80,** 472 (1983).
17. Oh, S. E., Fisher, G. B., Carpenter, J. E., and Goodman, D. W., *J. Catal.* **100,** 360 (1986).
18. Oh, S. H., and Eickel, C. C., *J. Catal.* **128,** 526 (1991).
19. Dubois, L. H., Hansma, P. K., and Somorjai, G. A., *J. Catal.* **65,** 318 (1980).
20. Vayenas, C. G., Bebelis, S., and Ladas, S., *Nature* **343** (6259), 625 (1990).
21. Vayenas, C. G., Bebelis, S., Yentekakis, I. V., and Lintz, H.-G., *Catal. Today* **11,** 303 (1992).
22. Yentekakis, I. V., and Vayenas, C. G., *J. Catal.* **111,** 170 (1988).
23. Vayenas, C. G., Bebelis, S., and Neophytides, S., *J. Phys. Chem.* **92,** 5083 (1988).
24. Bebelis, S., and Vayenas, C. G., *J. Catal.* **188,** 125 (1989).
25. Neophytides, S., and Vayenas, C. G., *J. Catal.* **118,** 147 (1989).
26. Vayenas, C. G., Bebelis, S., Neophytides, S., and Yentekakis, I. V., *Appl. Phys. A* **49,** 95 (1989).
27. Vayenas, C. G., Bebelis, S., Yentekakis, I. V., Tsiakaras, P., and Karasali, H., *Platinum Met. Rev.* **34,** 122 (1990).
28. Vayenas, C. G., and Neophytides, S., *J. Catal.* **127,** 645 (1991).
29. Vayenas, C. G., Bebelis, S., and Despotopoulou, M., *J. Catal.* **128,** 415 (1991).
30. Ladas, S., Bebelis, S., and Vayenas, C. G., *Surf. Sci.* **251/252,** 1062 (1991).
31. Vayenas, C. G., Bebelis, S., and Kyriazis, C., *Chem. Tech.* **21,** 500 (1991).
32. Vayenas, C. G., Bebelis, S., Yentekakis, I. V., and Neophytides, S., *Solid State Ionics* **53–56,** 97 (1992).
33. Bebelis, S., and Vayenas, C. G., *J. Catal.* **138,** 570, 588 (1992).
34. Tsiakaras, P., and Vayenas, C. G., *J. Catal.* **140,** 53 (1993).
35. Yentekakis, I. V., and Bebelis, S., *J. Catal.* **137,** 278 (1992).
36. Cavalca, C. A., Larsen, G., Vayenas, C. G., and Haller, G. L., *J. Phys. Chem.* **97,** 6115 (1993).
37. Alqahtany, H., Chiang, P., Eng, D., and Stoukides, M., *Catal. Lett.* **13,** 289 (1992).
38. Politova, T. I., Sobyanin, V. A., and Belyaev, V. D., *React. Kinet. Catal. Lett.* **41,** 321 (1990).
39. Mar'ina, O. A., and Sobyanin, V. A., *Catal. Lett.* **13,** 61 (1992).
40. Pritchard, J., *Nature* **343,** 592 (1990).
41. Yentekakis, I. V., Moggridge, G., Vayenas, C. G., and Lambert, R. M., *J. Catal.* **146,** 292 (1994).
42. Harkness, I. R., Yentekakis, I. V., Vayenas, C. G., and Lambert, R. M., in preparation.

43. Yentekakis, I. V., and Vayenas, C. G., *J. Catal.* **149,** 238 (1994).
44. Neophytides, S., Tsiplakides, D., Stonehart, P., Jaksic, M., and Vayenas, C. G., *Nature* **370,** 45 (1994).
45. Ladas, S., Kennou, S., Bebelis, S., and Vayenas, C. G., *J. Phys. Chem.* **97,** 8845 (1993).
46. Vayenas, C. G., Lee, B., and Michaels, J. N., *J. Catal.* **66,** 36 (1980).
47. Yentekakis, I. V., Neophytides, S., and Vayenas, C. G., *J. Catal.* **111,** 152 (1988).
48. Riekert, L., *Ber. Bunsenges. Phys. Chem.* **85,** 297 (1981).
49. Vöhrer, U., Ph.D. thesis, Universität Tübingen, 1992.
50. Yentekakis, I. V., and Vayenas, C. G., in preparation.
51. Schwab, G.-M., *Advan. Catal.* **2,** 251 (1950).
52. Cremer, E., *Advan. Catal.* **7,** 75, (1955).
53. Schwab, G.-M., *J. Catal.* **84,** 1 (1983).
54. Arakawa, T., Saito, A., and Shiokawa, J., *Chem. Phys. Lett.* **94,** 250 (1983); *Appl. Surf. Sci.* **16,** 365 (1983).
55. Boudart, M., and Djega-Mariadassou, G., "Kinetics of Heterogeneous Catalytic Reactions," pp. 121–122. Princeton Univ. Press, Princeton, NJ, 1984.
56. Pacchioni, G., and Vayenas, C. G., in preparation.